Earth and Planetary Science Letters 433 (2016) 232–240

Contents lists available at ScienceDirect

Earth and Planetary Science Letters

www.elsevier.com/locate/epsl

Experimental volcanic ash aggregation: Internal structuring of accretionary lapilli and the role of liquid bonding

Sebastian B. Mueller [a,*], Ulrich Kueppers [a], Paul M. Ayris [a], Michael Jacob [b], Donald B. Dingwell [a]

[a] Ludwig-Maximilians-Universität München (LMU), Earth and Environmental Sciences, Munich, Germany
[b] Glatt Ingenieurtechnik GmbH, Verfahrenstechnik, Weimar, Germany

ARTICLE INFO

Article history:
Received 5 August 2015
Received in revised form 4 November 2015
Accepted 6 November 2015
Available online 1 December 2015
Editor: T.A. Mather

Keywords:
volcanic ash
aggregation
accretionary lapilli
experimental volcanology
fluidized bed technology

ABSTRACT

Explosive volcanic eruptions can release vast quantities of pyroclastic material into Earth's atmosphere, including volcanic ash, particles with diameters less than two millimeters. Ash particles can cluster together to form aggregates, in some cases reaching up to several centimeters in size. Aggregation alters ash transport and settling behavior compared to un-aggregated particles, influencing ash distribution and deposit stratigraphy. Accretionary lapilli, the most commonly preserved type of aggregates within the geologic record, can exhibit complex internal stratigraphy. The processes involved in the formation and preservation of these aggregates remain poorly constrained quantitatively. In this study, we simulate the variable gas-particle flow conditions which may be encountered within eruption plumes and pyroclastic density currents via laboratory experiments using the *ProCell Lab System*® of Glatt Ingenieurtechnik GmbH. In this apparatus, solid particles are set into motion in a fluidized bed over a range of well-controlled boundary conditions (particle concentration, air flow rate, gas temperature, humidity, liquid composition). Experiments were conducted with soda-lime glass beads and natural volcanic ash particles under a range of experimental conditions. Both glass beads and volcanic ash exhibited the capacity for aggregation, but stable aggregates could only be produced when materials were coated with high but volcanically-relevant concentrations of NaCl. The growth and structure of aggregates was dependent on the initial granulometry, while the rate of aggregate formation increased exponentially with increasing relative humidity (12–45% RH), before overwetting promoted mud droplet formation. Notably, by use of a broad granulometry, we generated spherical, internally structured aggregates similar to some accretionary pellets found in volcanic deposits. Adaptation of a powder-technology model offers an explanation for the origin of natural accretionary pellets, suggesting them to be the result of a particular granulometry and fast-acting selective aggregation processes. For such aggregates to survive deposition and be preserved in the deposits of eruption plumes and pyroclastic density currents likely requires a significant pre-existing salt load on ash surfaces, and rapid aggregate drying prior to deposition or interaction with a more energetic environment. Our results carry clear benefits for future efforts to parameterize models of ash transport and deposition in the field.

1. Introduction

Volcanic ash, fragments of juvenile lava, crystals and/or older rock units less than two millimeters in diameter (Fisher, 1961), is produced in large quantities during explosive volcanic eruptions. Fine volcanic ash (particle diameter, $(p_d) < 63$ μm) can be distributed far away from the eruptive vent by ash transport processes, where it may cause a plethora of hazards and impacts (Dingwell et al., 2012). Under certain conditions within eruption plumes and pyroclastic density currents, ash particles can cluster together to form ash aggregates that range from micrometers to centimeters in size. Aggregates exhibit different aerodynamic properties than the individual ash grains which comprise them, promoting their 'premature' sedimentation from the plume and decreasing their residence time within the atmosphere, relative to the individual particles in isolation (Le Roux, 2014). Thus, ash aggregation may influence ash distribution (e.g., Folch et al., 2010) and deposit stratigraphy (e.g., Durant et al., 2009).

Ash aggregates can be characterized using the terminology of Brown et al. (2012); this prior study defined two classes of ash

* Corresponding author.
E-mail address: sebastian.mueller@min.uni-muenchen.de (S.B. Mueller).

http://dx.doi.org/10.1016/j.epsl.2015.11.007

aggregates, particle clusters (*PC*) and accretionary pellets (*AP*). Particle clusters are sub-divided into ash clusters (*PC1*) and coated particles (*PC2*), while *APs* can be divided into poorly-structured pellets (*AP1*), accretionary pellets (*AP2*) and liquid pellets (*AP3*). However, although field observations have evidenced the formation of all of these subtypes, the aggregates most commonly preserved within the geologic record tend to be *AP1* or *AP2*. The *AP1* aggregates are normally spherical or sub-spherical, ranging in diameter from several 100 µm to a few mm, and generally show poor internal structure. The *AP2* aggregates are similarly shaped, and can also grow to sizes of several mm; they consist of a relatively coarse grained core and (possibly several) fine grained rims.

The presence of the *AP1* and *AP2* aggregates in deposits evidences their comparative resilience to the highly energetic processes related to eruption dynamics and sedimentation processes. This preservation is not universal, as field studies have also documented shattered fragments of accretionary lapilli in deposits (Brown et al., 2010). However, our capacity to interpret the presence, absence and particular features (e.g., internal stratigraphy or granulometry) of aggregates within deposits as being indicative of particular eruption features or characteristics is limited. This stems from the absence of a quantitative understanding of the physical and/or chemical properties and in-plume boundary conditions which drive aggregate formation, disaggregation and the capacity of aggregates to survive deposition and be preserved in ash deposits.

The drivers on aggregate formation may relate to the mechanisms of both ash adhesion and aggregate growth. Particle adhesion is likely a product of three major forces, 1) electrostatic bonding, 2) Van der Waals forces and 3) liquid bonding. Although electrostatic charging of volcanic plumes is a well-known phenomenon (Lane and Gilbert, 1992; Cimarelli et al., 2013) that can lead to dry aggregation (e.g. Taddeucci et al., 2011; Del Bello et al., 2015), it is neglected in this study. With maximum surface charges of $\pm 10^{-5}$ C m^{-2} observed for particles in volcanic plumes (Gilbert et al., 1991), the electrostatic attraction and binding potential of ash particles is very low and even negligible in the presence of a liquid binder, as implied by experiments in fluidized beds with other particles (Randolph, 1988; Liu and Cameron, 2001; Saleh and Guigon, 2006). In order to build large ash aggregates stable enough to be preserved in the geologic record, we consider that liquid bonding may be the most important aggregation mechanism.

Previous in-field (Trusdell et al., 2005; Branney et al., 2008; Bonadonna et al., 2011), numerical (Costa et al., 2010; Folch et al., 2010) and laboratory studies (Gilbert and Lane, 1994; Schumacher and Schmincke, 1995; Van Eaton et al., 2012) have investigated the role of liquid bonding. Vibratory pan aggregation techniques, (Schumacher and Schmincke, 1995; Van Eaton et al., 2012) have successfully reproduced ash aggregates with characteristics (bulk diameter, density or granulometry) linearly dependent on humidity or wetting, until an 'overwetting' threshold was reached, whereafter, liquid 'mud' droplets (*AP3*) were formed (e.g. Gilbert and Lane, 1994). However, the influence of liquid bonding on ash aggregate formation remains only partially constrained. For example, although laboratory experiments have generated particle clusters (*PC*), the complex internal structures typical for *AP2* aggregates have yet to be reproduced. Furthermore, the effect of additional variables such as the surface tension and viscosity of the binding liquid (e.g. Kueppers et al., 2011), which in volcanic systems may be commonly comprised of condensates/solutions of co-erupted gases (e.g., $H_2O_{(g)}$, $SO_{2(g)}$, $HCl_{(g)}$, $HF_{(g)}$), have yet to be investigated.

The preservation of ash aggregates within ash deposits may be contingent on the establishment of strong interparticle binding mechanisms within the aggregate (e.g., cementation of solid bridges). Cementation may be driven by the interstitial precipitation of various sulphate and halide salts during the evaporation of the binding liquid. This process of cementation has been invoked following investigations of several field deposits (Tomita et al., 1985; Gilbert and Lane, 1994; Brown et al., 2010). The specific chemistry and abundance of these salts may depend both on the pH of the binding liquid and its capacity to dissolve or corrode the ash surface, and on the presence of pre-existing salts emplaced by higher temperature gas-ash interactions (cf. Witham et al., 2004; Ayris and Delmelle, 2012).

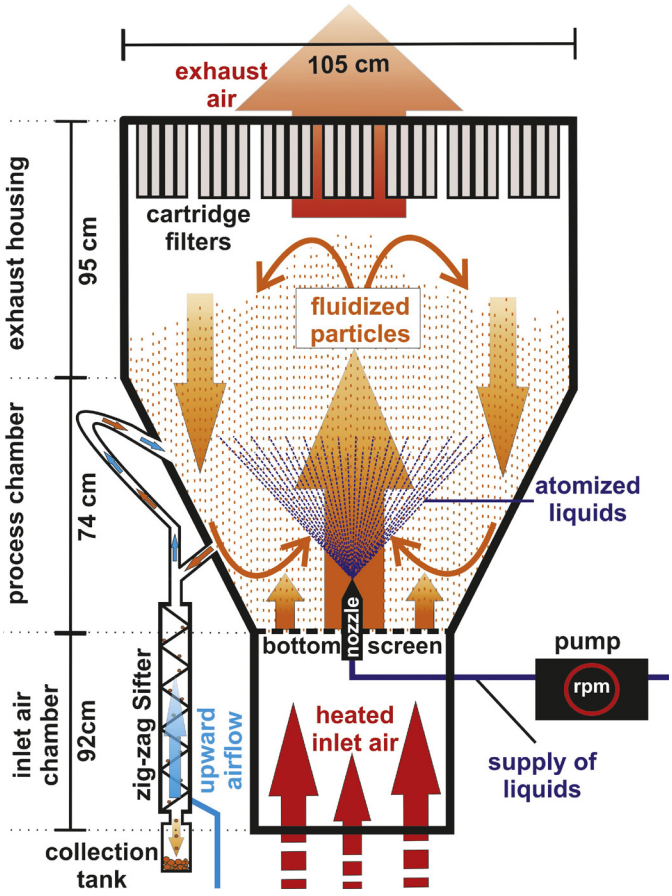

Fig. 1. Glatt ProCell® Lab System; solids are deposited on the bottom screen. Heated air flows from the inlet air chamber through the screen into the process chamber and drags particles upwards (fluidization). A nozzle in the center of the bottom screen sprays liquid into the fluidized particles. Liquid droplet size and spray rate are controlled manually. Topside cartridge filters separate fine particles from the exhaust air (exhaust chamber). Aggregates fall into the sifter through a contraflow air stream into a collection tank.

In this mechanistic study we present results of laboratory investigations on the formation and recovery of *AP1* and *AP2*-type ash aggregates. We investigated ash aggregation within fluidized beds, commonly utilized in industrial sectors, in particular in the food, animal feed, pharmaceutical, fertilizer, detergent and mineral processing industries, for investigation or generation of aggregates. Fluidized bed systems transform a granular material from a static (i.e. solid-like) to a dynamic (i.e. fluid-like) state, promoting aggregate formation under precisely-controlled conditions such as humidity, granulometry, air flow and temperature (Salman et al., 2006). In this study, we pioneer the use of this technology for our mechanistic investigation of volcanic ash aggregate formation, and provide new insights into the variables which permit the formation and survival of ash aggregates.

2. Methodology

For this study, we use the ProCell® Lab System (Fig. 1) by Glatt Ingenieurtechnik GmbH, Weimar, Germany. The ProCell® Lab

builds aggregates from fine powders, in this case, volcanic ash or soda-lime silicate glass beads. Solid particles are placed in a vessel and a stream of fluids passes up through the voids of the granular material. To generate a fluidized bed of particles, drag forces exerted by externally introduced fluids must exceed the weight of the particles. At a critical value of fluid velocity (the point of minimal fluidization velocity), the upwardly directed drag on particles will equalize the downwardly directed gravitational forces and maintain the particles in suspension. Above this minimal fluidization velocity, particles behave like a liquid and single particles follow stochastic streamlines (Salman et al., 2006). Within the fluidized bed, particles are wetted by a fine spray of liquid, promoting formation of liquid bridges between particles; aggregate growth is crucially controlled by operating conditions such as moisture, granulometry, process time, pneumatics or thermal conditions.

2.1. The ProCell® Lab System

The ProCell® Lab System consists of three parts (from bottom to top, see Fig. 1): the inlet air chamber, the process chamber and the exhaust housing. The Inlet air and process chamber are separated from each other by a bottom screen with a mesh size of 100 µm. An air stream is heated in the inlet air chamber and injected in the process chamber (*GF5* type, continuous fluidization) from below. The flow rate is sufficient to maintain the solid raw material in a fluidized state, while smaller particles which are lofted away from the bed by the airflow are captured within an installment of six cartridge filters. Overpressurized air is directed downwards through the cartridge filters every ten seconds, returning any trapped particles back to the fluidized bed. Liquids are injected into the *GF5* process chamber by a nozzle mounted on the bottom screen which directs its spray upwards, supplied by an external pump. Regulation of the pump allows supplying the process chamber with exactly the desired amount of liquid.

The ProCell® Lab is highly customizable in its operational conditions; the user may select the air flow through the process chamber (max. 250 $m^3\,h^{-1}$), the air flow temperature (max. 200 °C) and the pressure of the nozzle spraying the liquid (max. 6 bar). The instrument also maintains a constant record of air humidity and temperature in the process chamber.

The ProCell® Lab can either be run in batch or continuous mode; in the latter, a 'zig-zag-sifter' (Fig. 1) is installed at a product outlet, permitting aggregates to settle down into a collection tank. The sifter consists of a 30 cm long arrangement of steps, oriented with respect to each other at angles of 120°. An upward directed air flow (at 70–150 kPa overpressure) through the sifter prevents the collection of non-aggregated particles, forcing them to re-enter the fluidized bed. We also inspected the post-experiment particle bed within the process chamber, to determine whether any aggregates had survived within the fluidized bed.

2.2. Sample materials

In this mechanistic study of aggregation, we compared the behavior of two different materials. As an analogue material, we used spherical soda-lime glass beads (Kremer Pigmente, Germany, Table 1) in three granulometries, with p_d of <50 µm (fine), 40–70 µm (medium) and 150–210 µm (coarse). The beads show high abrasion resistance with only 1.6±0.1% weight loss per 100 h of grinding, ensuring a negligible change in granulometry during experiments. As a natural material, we used phonolitic volcanic ash (LS) from the Laacher See eruption (East Eifel volcanic field, Germany), with p_d of <40 µm (fine), 40–90 µm (medium) and 90–300 µm (coarse). Although the ash is approximately 13 ka old and cannot be considered chemically pristine, we consider the deposition and evaporation of salt solutions on the ash materials to be a physical process acting only on particle surfaces; accordingly, the Laacher See ash is utilized as a proxy for the more complex surface morphology of volcanic ash, relative to the glass beads.

Table 1
Chemical compositions, specific surface areas of selected granulometries, and densities of soda-lime silicate glass beads and Laacher See ash.

Oxides	Soda-lime glass beads (GB)[a]	Laacher See ash (LS)[b]
SiO_2 (wt%)	72	54.4
Al_2O_3 (wt%)	*minor*	20.1
Na_2O (wt%)	13	11.7
K_2O (wt%)	*minor*	5.6
CaO (wt%)	9	1.1
Fe_2O_3 (wt%)	–	1.8
FeO (wt%)	–	0.47
MgO (wt%)	*minor*	0.22
Specific surface area of granulometries[c]		
Fine	0.07 $m^2\,g^{-1}$	0.32 $m^2\,g^{-1}$
Medium	0.04 $m^2\,g^{-1}$	0.12 $m^2\,g^{-1}$
Coarse	0.02 $m^2\,g^{-1}$	0.07 $m^2\,g^{-1}$
Density	2500 $kg\,m^{-3}$[a]	2300 $kg\,m^{-3}$[d]

[a] Bulk chemistry and density provided by Kremer Pigmente GmbH, Germany.
[b] Bulk chemistry data from Wörner and Schmincke (1984).
[c] Surface areas measured with Camsizer® XT, Retsch GmbH, Germany.
[d] Density from ROTEC® GmbH & Co KG Rohstoff-Technik.

2.3. Salt-doping of ash materials

A H_2O–NaCl salt solution was selected for use in this experiment, in light of the extensive previous analysis of soluble salts on ash surfaces from multiple volcanoes via aqueous leaching, (see Witham et al., 2004; Ayris and Delmelle, 2012). These previous reviews noted that the most abundant elements in leachate solutions are Ca, Na, Mg, Cl and S, likely deriving from simple ionic sulphate and chloride salts (e.g., NaCl, $CaSO_4$).

The H_2O–NaCl solution, utilizing deionized H_2O, was sprayed at 7 $ml\,min^{-1}$ into the process chamber and over the fluidized LS ash or glass bead beds. The process chamber temperature was maintained at 50 °C and the solution was sprayed at a nozzle pressure of 100 kPa. The particles in the fluidized bed were therefore coated with a thin liquid layer, which rapidly evaporated, precipitating NaCl on the particle surfaces. Particle aggregation during the coating process was hindered by the low humidity of the heated atmosphere and slow spray rate of the solution. The efficiency of NaCl doping onto LS ash and glass beads was determined by comparison of the initial loading of NaCl dissolved into the sprayed solution, and the concentration on particle surfaces, which was determined by aqueous leaching. The leaching protocol utilized a solid:solution mass ratio of 1:10 and measured the effective NaCl concentration on particle surfaces via electrical conductivity measurements with an inoLab Cond 730®, manufactured by Wissenschaftliche Technische Werkstätten GmbH, Germany, calibrated using H_2O–NaCl solutions of known concentration.

The methods by which particles were coated with NaCl in the fluidized bed were both successful and reproducible. Twenty-five sub-samples were taken from a single NaCl-doping experiment and revealed a variation in NaCl concentration of less than 3%. The efficiency of doping, based on comparison of the initial mass of NaCl sprayed onto the ash materials, and the mass determined from post-experiment leachate analysis, was on the order of 90%. The loss likely reflects the loss of solution adhering to the internal surfaces of the process chamber.

2.4. Operational conditions

Our experiments were designed to (1) determine the critical concentration of NaCl and humidity needed to achieve artificial ash

Table 2
Summary of aggregation experiments carried out with the ProCell® Lab. Aggregation preservation is indicated as having occurred when (Y) when aggregates survived the impact into the collection tank.

Material	Particle diameter (µm)	Air flow (m^3/h)	Temperature (°C)	NaCl (mg/kg)	Aggregate preservation (Y/N)
Soda-lime glass	<50	50	90	1221	N
Soda-lime glass	<50	50	90	1774	Y
Soda-lime glass	<50	50	90	5021	Y
Soda-lime glass	<50	50	91	20312	Y
Soda-lime glass	40–70	60	89	1143	N
Soda-lime glass	40–70	60	92	2241	Y
Soda-lime glass	40–70	60	90	30231	Y
Soda-lime glass	40–70	60	91	49183	Y
Soda-lime glass	40–70	60	90	51563	Y
Soda-lime glass	150–210	80	89	1014	N
Soda-lime glass	150–210	80	90	2189	Y
Soda-lime glass	<50 + 150–210	80	90	1970	Y
Soda-lime glass	<50 + 150–210	80	90	4081	Y
Soda-lime glass	<50 + 150–210	80	92	16832	Y
Laacher See Ash	<40	40	90	2354	N
Laacher See Ash	<40	40	90	4286	N
Laacher See Ash	<40	40	91	5081	Y
Laacher See Ash	<40	40	89	16021	Y
Laacher See Ash	<40	40	90	30185	Y
Laacher See Ash	40–90	50	90	256	N
Laacher See Ash	40–90	50	90	1578	N
Laacher See Ash	40–90	50	90	4012	N
Laacher See Ash	40–90	50	90	5214	Y
Laacher See Ash	40–90	50	91	10743	Y
Laacher See Ash	40–90	50	90	13800	Y
Laacher See Ash	40–90	50	88	15214	Y
Laacher See Ash	40–90	50	91	48069	Y
Laacher See Ash	40–90	50	90	43000	Y
Laacher See Ash	<90	50	90	4912	Y
Laacher See Ash	<90	50	91	15023	Y
Laacher See Ash	90–300	60	93	4943	N
Laacher See Ash	90–300	60	87	14156	Y
Laacher See Ash	90–300	60	90	20145	Y
Laacher See Ash	90–300	60	90	47890	Y
Laacher See Ash	90–300	60	90	49102	Y
Laacher See Ash	<300	70	92	5145	N
Laacher See Ash	<300	70	90	15103	Y
Laacher See Ash	<300	70	89	30861	Y

aggregation in a fluidized bed, (2) constrain the influence of particle size on aggregation efficiency under controlled conditions (process chamber humidity, temperature etc.), and (3) generate internal structures similar to structures in natural *AP* samples (Brown et al., 2012).

Optimal aggregation conditions for fluidized particles of different densities and grainsizes with respect to air temperature, nozzle pressure and air flow inside the process chamber were experimentally constrained. Each individual experiment utilized 1 kg of the starting material and the inflow temperature T_{in} was set to 160 °C. This resulted in an average process chamber temperature T of 80 ± 15 °C, depending on the applied spray rate. For the aggregation experiment, nozzle pressure was set to 0.5 bar to allow larger water droplets to enter the fluidized bed, promoting the formation of a liquid film on solid particles within the fluidized bed. The airflow was set between 40 $m^3\,h^{-1}$ and 80 $m^3\,h^{-1}$, depending on particle size and type of material used. These conditions result in Reynolds numbers ranging between 8 and 28 for the ash experiments, applying equation (1):

$$Re = \frac{D_p V_s \rho}{(1-\varepsilon)\mu} \quad (1)$$

where Re is Reynolds Number, D_p is the equivalent spherical diameter of the particle, V_s is the superficial velocity, ρ is the density of the fluid, ε is the void fraction of the bed and μ is the dynamic viscosity of the fluid. The rising velocity of the air flow was 0.15 $m\,s^{-1}$–0.22 $m\,s^{-1}$, approximately two orders of magnitude lower than natural plume rising speeds (Tournigand et al., 2015).

3. Results

A total of 37 experiments were carried out to study the effect of selected aggregation media (glass beads or LS ash), granulometry, NaCl concentration, and relative humidity on aggregate shape, structure and preservation. The incidence of aggregate preservation in each of these experiments is documented in Table 2. As we observed no evidence for aggregate survival within the process chamber, we consider preservation to occur if aggregates were observed to enter the collection tank, rather than getting abraded and destroyed within the sifter. Notably, in all experiments where aggregation was recorded, aggregate arrival in the sifter was observed within a few seconds of the experiment onset.

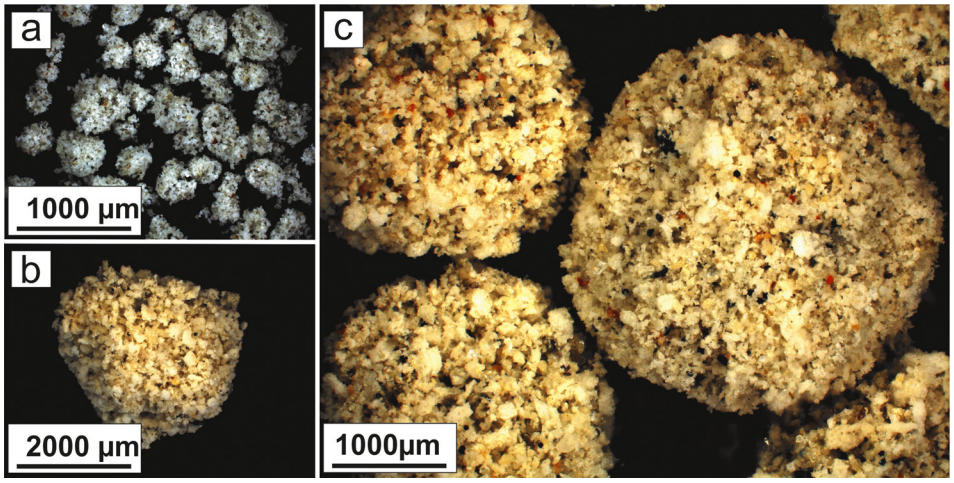

Fig. 2. (a), (b) and (c) show the transformation of aggregate shape from angular to (sub-) spherical. (a) shows aggregates that were produced from 40–90 µm LS ash. Broadening the granulometry to p_d of 40–300 µm (b), aggregates become sub-spherical. Adding a fine fraction ($p_d < 40$ µm) produces spherical aggregates (c). All images were produced using reflected light microscopy.

3.1. Effect of NaCl loading

In our experiment, aggregation occurs independently of surface salt concentration; during initial experiments using untreated glass beads and LS ash, and relative humidities of 10 and 20%, we observed the formation of aggregates ($p_d < 1000$ µm) which were destroyed within the sifter, rather than being preserved within the collection tank. The formation of stable aggregates which could be recovered from the collection tank could only be achieved using NaCl-coated glass bead and ash materials.

The minimum NaCl concentration required for recovery of aggregates comprised of glass beads with $p_d < 50$ µm was 1800 ± 54 mg kg^{-1}. For beads with initial p_d of 40–70 µm and 150–210 µm, the minimum NaCl concentration for recovery was 2200 ± 66 mg kg^{-1}. For LS ash, higher concentrations of NaCl were necessary for aggregate preservation within the sifter; approximately 5000 ± 150 mg kg^{-1} were needed to permit recovery of aggregates comprised of LS ash with $p_d < 40$ µm and <90 µm. Significantly higher NaCl concentrations were required when LS ash with p_d between 90 and 300 µm was used ($15\,103 \pm 453$ mg kg^{-1}). Additionally, we qualitatively observed that increasing NaCl concentrations on particle surfaces increased aggregate recovery from the collection tank. In aggregation experiments using glass beads of all grain sizes, coated with NaCl loadings of 2000 ± 60 mg kg^{-1}, we observed that 50% of aggregates which entered the collection tank disaggregated upon impact with its base, while no similar breakup was observed using beads coated with NaCl concentrations of $50\,000 \pm 1500$ mg kg^{-1}.

The maximum diameter of aggregates formed during $p_d <$ 50 µm glass bead experiments was one millimeter, an enlargement factor (EF) of 20 relative to the initial grain size, while aggregates comprised of 40–70 µm beads achieved an EF of 40. Notably, the EF for the 150–210 µm p_d fraction was approximately three; hence, the coarsest granulometry utilized in our experiments exhibited a limited capacity for aggregation, even at the highest NaCl concentrations. For the LS ash, much higher NaCl concentrations were necessary to achieve aggregation. The two ash fractions, fine and medium ($p_d < 40$ µm, 40–90 µm), required a minimum NaCl concentration of 5000 ± 150 mg kg^{-1} to aggregate with sufficient stability to survive the collection process. The large grained ash fraction ($p_d < 300$ µm) barely aggregated and required high NaCl concentrations ($20\,000 \pm 600$ mg kg^{-1}) to sediment as aggregates in the collection vessel. The EFs are 25 for fine, 35 for medium and 2 for coarse particles, respectively.

3.2. Effect of granulometry

In both glass bead and LS ash materials, changes in the granulometry of the starting material did not affect the minimum concentration of NaCl needed to permit the recovery of stable aggregates (2000 ± 60 mg kg^{-1} of NaCl for mixtures of glass beads with p_d of <50 µm and 150–210 µm; 5000 ± 390 mg kg^{-1} NaCl for mixtures of LS ash with p_d of 40–90 µm and 90–300 µm, and $15\,000 \pm 450$ mg kg^{-1} for LS ash with $p_d < 300$ µm). Over a range of NaCl concentrations up to $50\,000 \pm 1500$ mg kg^{-1}, we observed no effect on aggregation efficiency (mass of aggregates produced over time) in either material. However, changing granulometry did affect the shape of aggregates; with a narrow granulometry (e.g., $p_d < 40$ µm), aggregates were non-spherical, irregularly shaped and resembled un-structured particle clusters (*PC*), Fig. 2a. Broadening the initial granulometry by mixing two particle populations (e.g., 50:50 mixtures of particles with p_d of 40–90 µm and 90–300 µm or <40 µm and 40–90 µm) resulted in a transition in aggregate morphology from sub-spherical (Fig. 2b) to spherical (Fig. 2c). Fluidized beds comprised of glass beads with p_d of <50 µm and 150–210 µm produced aggregates with accumulations of coarse particles ($p_d > 150$ µm) in their core and fine particles in their rims (Fig. 3a). Additionally, solid NaCl bridges were clearly visible connecting particles with each other (Fig. 3b). Similarly, for LS ash aggregates, internal structuring was enhanced by broadening the starting granulometry (Fig. 4); while a separation between core and rim was not readily observed in aggregates comprised of LS ash with $p_d < 40$ µm (Fig. 4a), the cores became coarser grained than the rims for aggregation experiments using LS ash with $p_d < 90$ µm (Fig. 4b) and $p_d < 300$ µm (Fig. 4c).

3.3. Effect of humidity

The effect of humidity on aggregation preservation was also measured (Fig. 5). As no influences on aggregate recovery other than of surface area were implied from previous experiments on glass beads and LS ash, we confined our investigation of humidity to one material only (LS ash). We performed three experimental series utilizing NaCl loadings of $15\,000 \pm 450$ mg kg^{-1} on i) LS ash with $p_d < 40$ µm, ii) LS ash with p_d 40–90 µm, and iii) a 50/50 ratio of these two granulometries.

Changing the relative humidity of the air within the system changed the rate of aggregate production. Aggregation initiated, depending on the starting granulometry, between 12 and 18% RH.

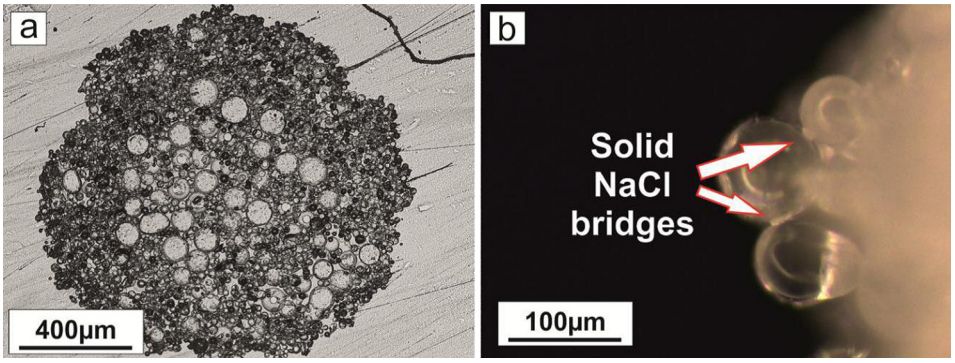

Fig. 3. a) Cross section through an experimentally generated glass bead aggregate, produced after impregnating with epoxy resin. The starting granulometry in the experiment consisted of particles with $p_d < 50$ µm and $p_d = 150$–210 µm glass beads. Coarse glass beads are predominantly found in the core region, while fine particles are principally located on the outside of the aggregate. b) Image showing solid NaCl bridges connecting glass beads ($p_d = 40$–70 µm) of an aggregate. All images were produced using reflected light microscopy.

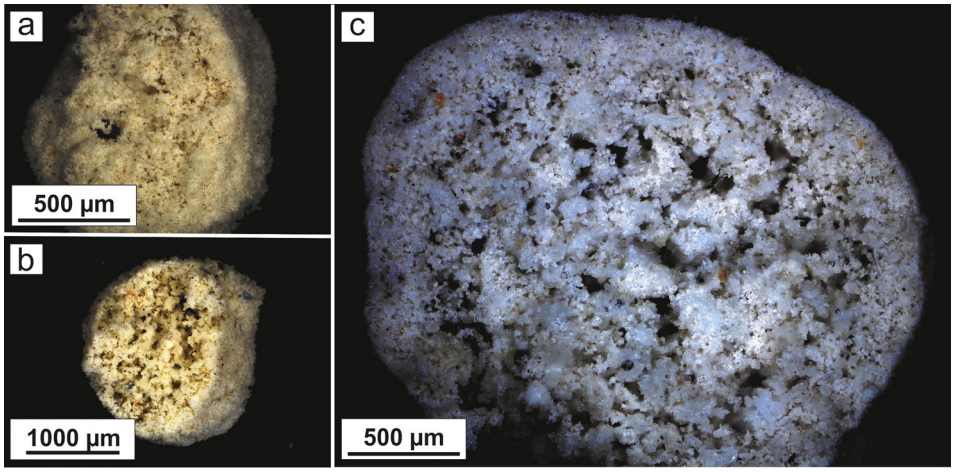

Fig. 4. a)–c) Cross sections showing the increasing evidence of internal aggregate structuring depending on the starting granulometry; a) consists of LS ash with $p_d < 40$ µm – internal stratification is not detected. b) consists of LS ash with $p_d < 90$ µm and c) of LS ash with $p_d < 300$ µm. In c), coarse grained particles ($p_d > 100$ µm) are concentrated in the center whereas fine grained particles are densely packed in the rim of the aggregate. All images were produced using reflected light microscopy.

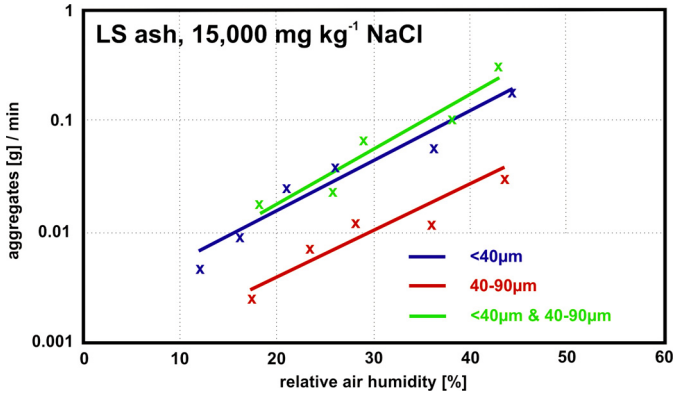

Fig. 5. The influence of humidity on mass production of preserved aggregates [g] per minute is shown for various granulometries. The highest rate of aggregate production is demonstrated when using a broad granulometry of starting material ($p_d < 40$ and 40–90 µm), followed by the $p_d < 40$ µm and the p_d 40–90 µm charge. NaCl concentration is at 15 000 mg kg^{-1}.

The number of aggregates produced per minute increased exponentially up to 45% RH. Most aggregates are produced when the grain size distribution of the starting material is broad (50/50 mix of LS ash with $p_d < 40$ µm and 40–90 µm). The lowest production rate of aggregates is achieved by particles with p_d of 40–90 µm, used in isolation. These data evidence a significant control of humidity on aggregation rate. The upward directed airflow within the sifter dried the aggregates during transit, such that residual internal moistures were below 1 wt%. However, at approximately 50% RH, the upward directed airflow in the sifter was insufficient to dry aggregates, resulting in the accumulation of a heap of wet ash in the collection tank, rather than dry, coherent aggregates.

4. Discussion

4.1. Agreement with previous studies

During our experiments, we observed the formation of aggregates with clear internal structuring. LS aggregates from initial materials with $p_d < 300$ µm, have a modal p_d of 63 µm over the whole particle, but within their rims, the modal p_d is 12 µm. These aggregates show many similarities with *AP2* aggregates found in nature; in studies of natural ash aggregates, the dominant particle size fraction (90 vol%) has $p_d < 60$ µm, while the largest particles found in natural aggregates have p_d of ~200–500 µm (Sheridan and Wohletz, 1983; Cole et al., 2002; Bonadonna et al., 2002; Trusdell et al., 2005; Cunningham and Beard, 2014; Scolamacchia and Dingwell, 2014). Within internally structured natural ash aggregates, coarser particles are enriched in the core, while finer particles comprise the rim (Brown et al., 2012). For example, Scolamacchia and Dingwell (2014) analyzed ash aggregates from the 1982 El Chichon eruption (Mexico); the cores of these aggregates consisted of coarser material ($p_d = 63$–250 µm) while their rims contained finer-grained particles ($p_d < 63$ µm) with ~75% of

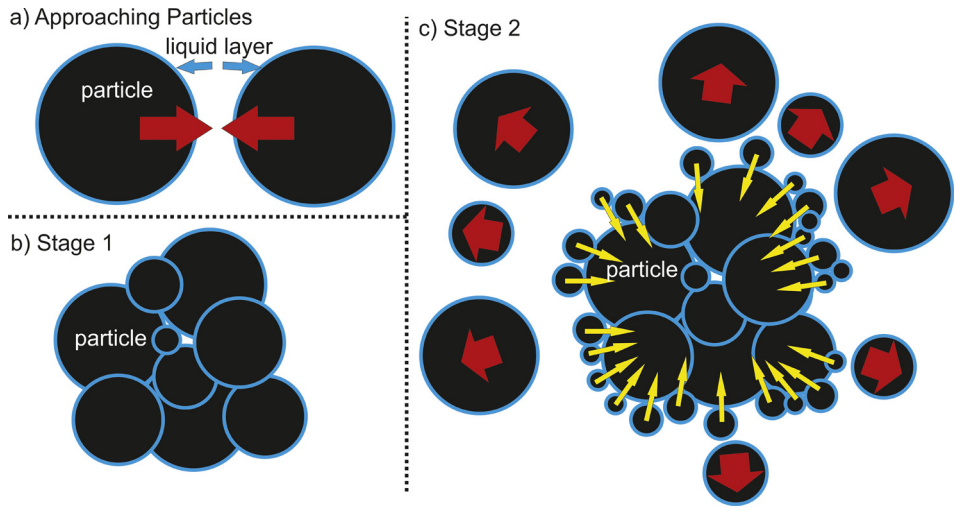

Fig. 6. Illustration of the Ennis et al. (1991) model: in a) two particles with a liquid layer of the thickness h are approaching each other. b) reflects the non-inertial regime of aggregate growth in which all particles stick after collision due to viscous and elastic forces sufficiently dissipating kinetic collision energies. c) shows the inertial regime, where aggregate growth in which viscous Stokes number and critical viscous Stokes number are approximately equal. Small particles stick to the existing aggregate due to lower collision energies. Large particles rebound due to higher collision energies; rebound forces cannot be dissipated by liquid bonding forces. The non-inertial regime builds the core of an accretionary pellet, reflecting the total particle size range, while the inertial regime builds up the fine grained rim.

rim grains smaller than 16 μm in diameter. In addition to their structural similarities, the aggregates formed in our experiments exhibit comparable densities to natural samples; the density of the experimental aggregates (480 kg m^{-3}) is within the range of values reported for ash aggregates recovered by Taddeucci et al. (2011) from the 2010 Eyjafjallajökull eruption (100 to 1000 kg m^{-3}).

Our experiments are also in good agreement with previous studies which identify liquid bonding as a primary control on the formation of AP aggregates. We observed a clear dependency of aggregate accumulation rate in the collection tank on RH, with an exponential increase between 12 and 45% RH (5–19 wt% H_2O at 90 °C). At lower values, no aggregates were observed in the sifter. At higher humidity, overwetted aggregates coalesced in the collection tank and formed a heap of wet ash (Fig. 5). The range of humidity values observed is in good agreement with natural observations and other experimental studies; Tomita et al. (1985) observed pellet fallout during eruptions at Sakurajima Volcano (Japan) and described ash aggregation solely on days with RH of >18% at a height of 4 km, corresponding to the maximum plume height. In laboratory experiments, Schumacher and Schmincke (1995) determined that the optimum quantity of water to promote aggregation of ash within a pan was between 15–25 wt%. In similar experiments, utilizing a vibratory pan, Van Eaton et al. (2012) determined that aggregation was most efficient at liquid concentrations between 10–15 wt%, while at higher concentrations, slurries rather than aggregates, were formed. Based on the good agreement of our experimental data and previous studies, we conclude that the concentration of liquids during aggregation controls the number of particle aggregates produced; with increasing liquid binder concentration, aggregate production increases exponentially (Fig. 5).

The process of cementation of aggregates has been described several times for natural deposits, invoking the role of salts as binding agents, but quantification of the related process has not yet been achieved. In our study, although we observed aggregation under all conditions, including NaCl-free particles, we required high NaCl loadings (>5000 mg kg^{-1}) to permit recovery of stable ash aggregates from the collection tank. Higher loadings of NaCl were required to promote recovery of LS ash aggregates, compared to that required for glass bead aggregates. This likely reflects the complex morphology, and accordingly, greater surface area, of the LS ash (Table 1); to achieve the same salt loading per unit surface area required a greater dose of salts per unit mass in the LS ash, relative to the glass beads. It is not yet known whether the behavior of NaCl is salt-specific, or applicable to all soluble salts on ash surfaces. If the latter, it is notable that the total loading of soluble salts utilized in this study, while high, remain within the range of concentrations implied by previous leachate studies: data summarized by Ayris and Delmelle (2012) yielded both a calculated mean and median sulphate and chloride salt loading on the order of 6000 mg kg^{-1}, with maximum values in excess of 20 000 mg kg^{-1} being reported in some scenarios. Additionally, preparatory to the current study, we disaggregated and subsequently leached fragile accretionary pellets recovered from deposits of the 2011 dome collapse at Soufrière Hills Volcano (Montserrat). The total concentration of Ca, Cl, Mg, Na and S in leachate solutions (1:100 ash:water ratio, 4 hour leaching time), indicative of total surface salt loading, was in excess of 5000 mg kg^{-1}.

4.2. A new perspective on ash aggregate formation

Our findings have demonstrated that experiments utilizing fluidization bed techniques can produce aggregates of comparable structure and under comparable conditions to those previously observed both in experimental studies and field investigations. Crucially, this realization of comparability opens a new avenue of research in the application of existing industrial studies to volcanic systems.

Ennis et al. (1991) have previously proposed a particle coalescence model derived from industrial particle aggregation studies, which can be utilized to explain our experimental results, and by analogy, the formation of ash aggregates during explosive eruptions. The model is based on the assumption that two approaching particles with a liquid film layer (Fig. 6a) of thickness h coalesce after collision, when the initial kinetic energy is dissipated through viscous and elastic losses. Liquid layers of the two particles will have first contact at a distance $2h$. Viscous losses are calculated by using results for Stokes flow between two approaching particles. The coefficient of restitution e dissipates energy within the solid phase. Resulting calculations show that particles will coalesce when the viscous Stokes number St_v (eq. (2)) is less than some critical viscous Stokes number St_v^* (eq. (3)):

$$St_v = \frac{4\rho u_0 p_d}{9\mu} \quad (2)$$

$$St_v^* = \left(1 + \frac{1}{e}\right) \ln\left(\frac{h}{h_a}\right) \quad (3)$$

where ρ is the particle or aggregate density, u_0 is half the initial relative velocity of the impact, p_d is the particle or aggregate diameter, μ is the liquid viscosity and h_a is the characteristic height of surface asperities. St_v describes the ratio of initial kinetic energy to energy dissipated by viscous effects. St_v will increase during the aggregation process since the aggregate grows.

The interplay of the various parameters in this theoretical model allow for the constraint of three granulation stages which describe the growth of both experimental and natural accretionary pellets. After Ennis et al. (1991), the first stage is referred to as the non-inertial regime ($St_v \ll St_v^*$), where collisions between particles of all sizes are successful. In this stage, a large range of particle sizes will stick together (e.g. $p_d < 300$ μm in the ProCell® Lab experiments), producing a coarse-grained (reflecting the whole size range of available particles), porous core. In the second granulation stage (inertial regime), the viscous Stokes number St_v is approximately equal to the critical Stokes number St_v^*. Coalescence now depends on the size of colliding particles, whereby collisions between two small, or one small and one large particle(s), keeps St_v low and enables coalescence, while collisions between two big particles, e.g. an aggregate and a large ash grain, causes high St_v and hinders coalescence. In the inertial regime, only smaller particles will stick to existing aggregates due to the increasing difference in diameter, the likelihood of increasing impact velocities, and the increasing St_v number. In the third granulation stage, St_v is greater than St_v^* and collisions do not permit coalescence. In this generalized model, the initial particle size distribution is likely an important control; with a narrow granulometry, any aggregate structuring effects imparted during the different regimes are likely minimal, producing a poorly structured ash pellet (*AP1*). In contrast, with a broader initial particle size distribution, aggregate growth would produce an internally structured clast with a dense, fine-grained rim (*AP2*). It is also possible that pre-inertial regime interruption of aggregation processes via sedimentation into particle-poor environments could favor the formation of *AP1*, rather than *AP2* aggregates.

The Ennis model (1991) can also explain the increasing rate of aggregation with increasing air humidity, prior to overwetting (Fig. 5). The increasing quantity of liquid sprayed into the process chamber increases the liquid layer thickness h on single particles; in our experiments using LS ash with $p_d < 40$ μm, increasing RH from 12 to 45% is calculated to increase h from 160 to 590 nm. Increasing h values increase St_v^*, allowing more particles to coalesce, and increasing the rate of aggregate production. The initiation of aggregation at lower humidity for fine grain sizes (Fig. 5) can also be explained; smaller particle diameters, p_d, result in lower impact velocities u_0 and an overall smaller St_v, another criterion for enhanced aggregation. A further implication for liquid bonding from the Ennis model (1991) is a dependence on liquid viscosity; while our experiments used only deionized water, the condensation or emplacement of fluids of different viscosities (e.g., liquid sulphur, Scolamacchia and Dingwell, 2014) on ash surfaces may significantly influence aggregation processes.

Observations from our experiments offer a number of further insights into the formation of *AP* aggregates. The arrival of aggregates within the collection tank at the start of the experiment was near-instantaneous; this suggests that the rims of *AP* aggregates, rather than being formed by transport through a finer-grained particle suspension than that from which the core was constructed, can formed rapidly from the same particle population that builds the initial core via a selective aggregation process. The fragility of salt-free or salt-poor aggregates in our experiments further suggests that a continuous cycle of collisions, aggregation and disaggregation may occur in eruption plumes and pyroclastic density currents (PDC), but that once specific boundary conditions are achieved, rapid growth of structured aggregates is possible. The low experimental Reynolds numbers of our study (8–28), relative to those of e.g., PDCs (10^6–10^9, e.g. Andrews and Manga, 2012) suggests that one environment where these conditions are achieved could be the most dilute parts of PDCs, lofted co-pyroclastic plumes or the umbrella regions of eruption plumes. However, such conditions are unlikely to be the only regimes where aggregate growth is promoted.

Given the apparent fragility of many of the aggregates formed in our experiments, the capacity of *AP* aggregates to survive deposition and be preserved within a deposit likely requires the establishment of strong interparticle bridges to strengthen it. This may be particularly important if the aggregate traverses a more energetic region of an eruption plume or PDC after formation but prior to deposition. Salt-driven cementing would require not only an abundance of pre-existing soluble salts, but also rapid drying after formation. This was illustrated in our experiments; the lower humidity within the sifter promoted liquid evaporation and salt precipitation, but the absence of aggregates in the post-experiment process tank suggests that fluidized bed collapse in still-humid conditions prevented drying and favored aggregate breakup. Within volcanic settings, lower humidity conditions could be achieved via numerous mechanisms, e.g., by sedimentation into drier atmospheres from a water-rich plume, or the recycling of aggregates from cold regions of the plume and/or PDC into hotter regions (>100 °C). Thus, much as there may be multiple environments where aggregate growth is favored, there may be multiple conditions where salt-driven cementing may stabilize those aggregates.

5. Conclusion

Accretionary pellets were produced successfully in the laboratory by using fluidization bed techniques. Liquid bonding forces promoted particle adhesion following collisions, building aggregates up to 1000 μm in size. These aggregates were fragile and were easily disaggregated, but when the initial particle mass was coated with NaCl, could be stabilized by the dissolution and reprecipitation of NaCl as solid interparticle bridges. High, but volcanically relevant (~2000 mg kg^{-1}) concentrations of surface salts enabled recovery of some aggregated particles, while increasing salt loads promoted increased stability and improved aggregate preservation. The granulometry of the initial particle mass had a strong influence on the growth and structure of aggregates; fine-grained particles ($p_d < 100$ μm) grew up to 40 times larger than the original diameter of the starting material, while coarse particles reached final diameters of only three times that of the initial particle. Similar to the results of previous field studies and experimental observations, aggregate formation occurred within a discrete range of humidities; in our experiment, aggregates formed above 12% RH, and disaggregated into a mud or slurry at humidities greater than 45% RH.

Most notably, through the use of particle populations with broad granulometries, we generated (sub-) spherical and internally structured aggregates with coarse grained cores and fine grained rims, similar to natural *AP2* aggregates observed in volcanic deposits. Applying a numerical model derived from industrial particle aggregation studies, we conclude that shape and internal structuring of aggregates is controlled by the initial granulometry, mediated by a fast-acting selective aggregation process. In so doing, we offer a generalized model for the formation of both *AP1* and *AP2* aggregates, which also identifies the importance of the concentration, and perhaps viscosity, of the liquid binding agent which facilitates aggregation. Our findings suggest that aggregation and disaggregation processes occur in all volcanic environments, but

that once specific boundary conditions are achieved, growth of *AP* aggregates is rapid. To preserve these aggregates upon deposition may further require a high loading of pre-existing surface salts, and a pre-deposition transition from a high to low humidity environment. Although further constraints on the parameters which drive both aggregation and cementation are required, the findings of this paper should be considered as a valuable input into numerical aggregation and ash dispersal models.

Acknowledgements

We thank Ulrich Walter, Melanie Guttzeit and Katja Oppermann for their help during the fluidized bed experiments at Glatt Industries. We thank Corrado Cimarelli, Jacopo Taddeucci, Stefano Alois and Costanza Bonadonna for fruitful discussions. The Laacher See ash used in this study was kindly offered by ROTEC GmbH & Co. KG (Mühlheim–Kärlich, Germany). This work is supported by the Marie Curie Initial Training Network 'VERTIGO', funded through the European Seventh Framework Programme (FP7 2007–2013) under Grant Agreement number 607905. P.A. and D.B.D. acknowledge the support of European Research Council Advanced Grant 247076 "EVOKES" (Explosive volcanism in the Earth System). This manuscript benefited from constructive comments of Stephen J. Lane, Sebastian Watt and the editor Tamsin A. Mather.

References

Andrews, B.J., Manga, M., 2012. Experimental study of turbulence, sedimentation, and coignimbrite mass partitioning in dilute pyroclastic density currents. J. Volcanol. Geotherm. Res. 225–226, 30–44. http://dx.doi.org/10.1016/j.jvolgeores.2012.02.011.

Ayris, P.M., Delmelle, P., 2012. The immediate environmental effects of tephra emission. Bull. Volcanol. 74, 1905–1936.

Bonadonna, C., Genco, R., Gouhier, M., Pistolesi, M., Cioni, R., Alfano, F., Hoskuldsson, A., Ripepe, M., 2011. Tephra sedimentation during the 2010 Eyjafjallajökull eruption (Iceland) from deposit, radar and satellite observations. J. Geophys. Res. 116, B12202.

Bonadonna, C., Calder, E.S., Choux, C., Jackson, P., Lejeune, A.M., Loughlin, S., Mayberry, G.C., Norton, G., Rose, W.I., Ryan, G., Sparks, R.S.J., Young, S.R., 2002. Tephra fallout from the eruption of Soufriere Hills Volcano, Montserrat. In: Druitt, T.H., Kokelaar, B.P. (Eds.), The Eruption of Soufriere Hills Volcano, Montserrat, from 1995–1999. In: Geological Society of London Memoir, vol. 21, pp. 483–516.

Branney, M.J., Bonnichsen, B., Andrews, G.D.M., Ellis, B., Barry, T.L., McCurry, M., 2008. Snake River SR-type volcanism on the Yellowstone hotspot track: distinctive products of unusual high-temperature silicic super-eruptions. Bull. Volcanol. 79, 293–314.

Brown, R.J., Branney, M.J., Maher, C., Dávila-Harris, P., 2010. Origin of accretionary lapilli within ground-hugging density currents: evidence from pyroclastic couplets on Tenerife. Geol. Soc. Am. Bull. 122, 305–320. http://dx.doi.org/10.1130/B26449.1.

Brown, R.J., Bonadonna, C., Durant, A.J., 2012. A review of volcanic ash aggregation. Phys. Chem. Earth 45–46, 65–78. http://dx.doi.org/10.1016/j.pce.2011.11.001.

Cimarelli, C., Alatorre-Ibargüengoitia, M.A., Kueppers, U., Scheu, B., Dingwell, D.B., 2013. Experimental generation of volcanic lightening, Geology. http://dx.doi.org/10.1130/G34802.1.

Cole, P.D., Calder, E.S., Sparks, R.S.J., Clarke, A.B., Druitt, T.H., Young, S.R., Herd, R.A., Harford, C.L., Norton, G.E., 2002. Deposits from the dome-collapse and fountain-collapse pyroclastic flows at Soufriere Hills Volcano, Montserrat. Mem. Geol. Soc. Lond. 21, 231–262.

Costa, A., Folch, A., Macedonio, G., 2010. A model for wet aggregation of ash particles in volcanic plumes and clouds: 1. Theoretical formulation. J. Volcanol. Geotherm. Res. 115, B09201. http://dx.doi.org/10.1029/2009JB007175.

Cunningham, J.K., Beard, A.D., 2014. An unusual occurrence of mafic accretionary lapilli in deep-marine volcaniclastics on Eua, Tonga: palaeoenvironment and process. J. Volcanol. Geotherm. Res. 274, 139–151.

Del Bello, E., Taddeucci, J., Scarlato, P., Giacalone, E., Cesaroni, C., 2015. Experimental investigation of the aggregation–disaggregation of colliding volcanic ash particles in turbulent, low-humidity suspensions. Geophys. Res. Lett. 42. http://dx.doi.org/10.1002/2014GL062292.

Dingwell, D.B., Lavallée, Y., Kueppers, U., 2012. Volcanic ash: an agent in Earth systems. Phys. Chem. Earth, Part A, Solid Earth Geod. 45–46, 2–4.

Durant, A.J., Rose, W.I., Sarna-Wojcicki, A.M., Carey, S., Volentik, A.C., 2009. Hydrometeor-enhanced tephra sedimentation from the 18 May 1980 Mount St. Helens (USA) volcanic cloud. J. Geophys. Res. 114 (B3). http://dx.doi.org/10.1029/2008JB005756.

Ennis, B.J., Tardos, G., Pfeffer, R., 1991. A microlevel-based characterization of granulation phenomena. Powder Technol. 65, 257–272.

Fisher, R.V., 1961. Proposed classification for volcaniclastic sediments and rocks. Geol. Soc. Am. Bull. 72, 1409–1414.

Folch, A., Costa, A., Durant, A., Macedonio, G., 2010. A model for wet aggregation of ash particles in volcanic plumes and clouds: 2. Model application. J. Geophys. Res. 115, 1–16.

Gilbert, J.S., Lane, S.J., Sparks, R.S.J., Koyaguchi, T., 1991. Charge measurements on particle fallout form a volcanic plume. Nature 349, 598–600.

Gilbert, J.S., Lane, S.J., 1994. The origin of accretionary lapilli. Bull. Volcanol. 56, 398–411.

Kueppers, U., Auer, B., Cimarelli, C., Scolamacchia, T., Dingwell, D.B., 2011. Experimentally constraining the boundary conditions for volcanic ash aggregation. Geophys. Res. Abstr. 13, EGU2011–EGU11999.

Lane, S.J., Gilbert, J.S., 1992. Electric potential gradient changes during explosive activity at Sakurajima volcano. Bull. Volcanol. Soc. Jpn. 54, 590–594.

Le Roux, J.P., 2014. Fall velocity of multi-shaped clasts. J. Volcanol. Geotherm. Res. 289, 130–139.

Liu, Y., Cameron, I.T., 2001. A new wavelet-based method for the solution of the population balance equation. Chem. Eng. Sci. 56, 5283–5294. http://dx.doi.org/10.1016/S0009-2509(01)00196-8.

Randolph, A.D., 1988. Theory of Particulate Processes: Analysis and Techniques of Continuous Crystallization, second edn. Academic Press, San Diego.

Saleh, K., Guigon, P., 2006. Coating and encapsulation processes in powder technology. In: Salman, A.D., Hounslow, M.J., Seville, J.P.K. (Eds.), Handbook of Powder Technology – Granulation, eleventh edn. Elsevier, Amsterdam.

Salman, A.D., Hounslow, M.J., Seville, J.P.K., 2006. Handbook of Powder Technology – Granulation, eleventh edn. Elsevier, Amsterdam.

Schumacher, R., Schmincke, H.-U., 1995. Models for the origin of accretionary lapilli. Bull. Volcanol. 56, 626–639.

Scolamacchia, T., Dingwell, D.B., 2014. Sulfur as a binding agent of aggregates in explosive eruptions. Bull. Volcanol. 76, 871–883.

Sheridan, M.F., Wohletz, K.H., 1983. Origin of accretionary lapilli from the Pompeii and Avellino deposits of Vesuvius. In: Gooley, Ron (Ed.), Microbeam Analysis. San Francisco Press, Inc.

Taddeucci, J., Scarlato, P., Montanaro, C., Cimarelli, C., Del Bello, E., Freda, C., Andronico, D., Gudmudsson, M.T., Dingwell, D.B., 2011. Aggregation-dominated ash settling from the Eyjafjallajökull volcanic cloud illuminated by field and laboratory high-speed imaging. Geology 39, 891–894.

Tomita, K., Kanai, T., Kobayashi, T., Oba, N., 1985. Accretionary lapilli formed by the eruption of Sakurajima Volcano. J. Jpn. Assoc. Miner. Petrol Econ. Geo. 80, 49–54.

Tournigand, P.Y., Taddeucci, J., Scarlato, P., Gaudin, D., Del Bello, E., 2015. Field-based study of volcanic ash via visible and thermal high-speed imaging of explosive eruptions. Geophys. Res. Abstr. 17, EGU2015–EGU12553.

Trusdell, F.A., Moore, R.B., Sako, M., Randall, A.W., Koyanagi, S.K., Chong, R., Camacho, J.T., 2005. The 2003 eruption of Anatahan Volcano, commonwealth of the Northern Mariana Islands: chronology, volcanology, and deformation. J. Volcanol. Geotherm. Res. 146, 184–207.

Van Eaton, A.R., Muirhead, J.D., Wilson, C.J.N., Cimarelli, C., 2012. Growth of volcanic ash aggregates in the presence of liquid water and ice: an experimental approach. Bull. Volcanol. 74, 1963–1984. http://dx.doi.org/10.1007/s00445-012-0634-9.

Witham, C.S., Oppenheimer, C., Horwell, C.J., 2004. Volcanic ash leachates: a review and recommendations for sampling methods. Volcanol. Geotherm. Res. http://dx.doi.org/10.1016/j.jvolgeores.2004.11.010.

Wörner, G., Schmincke, H.-U., 1984. Mineralogical and chemical zonation of the Laacher See Tephra Sequence (East Eifel W. Germany). J. Petrol. 25, 805–835. http://dx.doi.org/10.1093/petrology/25.4.805.